

Communication

# Dispersion Engineering of Waveguide Microresonators by the Design of Atomic Layer Deposition

Pei-Hsun Wang \* , Nien-Lin Hou and Kung-Lin Ho

Department of Optics and Photonics, National Central University, Taoyuan City 32001, Taiwan

\* Correspondence: phwang@dop.ncu.edu.tw

**Abstract:** In this work, we demonstrate dispersion engineering of silicon nitride waveguide resonators with atomic layer deposition (ALD). We conducted theoretical and experimental analyses on the waveguide dispersion with air cladding, hafnium oxide ( $\text{HfO}_2$ ) cladding, and aluminum oxide ( $\text{Al}_2\text{O}_3$ ) cladding. By employing ALD  $\text{HfO}_2$  as the cladding layer, the dispersion of waveguide can be tuned to a finer degree in the normal regime at a wavelength of 1550 nm. On the other hand, using ALD  $\text{Al}_2\text{O}_3$  cladding provides the waveguide dispersion that spans regimes in normal, near-zero, and anomalous dispersion.

**Keywords:** group velocity dispersion; optical waveguide; dispersion engineering; atomic layer deposition; microresonator

## 1. Introduction

Group-velocity dispersion (GVD) of optical waveguides plays a significant role in applications from optical fibers [1,2] to integrated waveguides [3,4]. For linear photonics applications, such as optical communication, the waveguide dispersion impacts the capacity limits of optical fiber networks [5]; as for nonlinear optics, the initiation of nonlinear mechanism strongly correlates with the dispersion regimes [2,4,6]. The waveguide geometries are able to provide dispersion tuning in a large range, making them beneficial for accommodating different applications. Normal to anomalous dispersion tuning can be achieved by adjusting the dimension of the waveguide core [6,7]. Additionally, accurate control of GVD is a crucial task for numerous photonic applications. For instance, several studies show near-zero dispersion by properly designing the waveguide geometry of core materials, such as silicon nitride (SiN) [6–8], arsenic tri-sulfide ( $\text{As}_2\text{S}_3$ ) [9], or hybrid silicon/silicon nitride layers [10]. However, for traditional fabrication processes, waveguide dimensions are typically realized through a combination of deposition, lithographic patterning, and etching. Achieving precise control of the waveguide dimension can be challenging, which makes it difficult to design waveguides with the desired dispersion. For example, anomalous dispersion of SiN waveguides can be achieved by tailoring the height above 700 nm, in which strain-induced cracks need to be avoided using pre-etched trenches [7,11,12] or cycling deposition [13]. Moreover, this approach determines the waveguide dispersion at a very early stage, and limits the flexibility to adjust dispersion for individual devices. Recently, a few studies demonstrated the possibility to tune or reconstruct waveguide dispersion by a patternable polymer cladding layer [14]. Although the dispersion can be well-tuned in a large range in the final stage of fabrication, this method relies on spinning polymer cladding, and may not allow precise tuning due to limitations in the fabrication process. Compared to the uniformity and roughness issue of a polymer cladding, thin film coating, especially for atomic layer deposition (ALD), provides ultimate uniformity and accurate thickness control. Traditionally, ALD layers have been used to improve the surface roughness and mitigate the waveguide loss [15]. In addition to improving waveguide quality, modifying the confined mode by ALD layers also provides another degree of



**Citation:** Wang, P.-H.; Hou, N.-L.; Ho, K.-L. Dispersion Engineering of Waveguide Microresonators by the Design of Atomic Layer Deposition. *Photonics* **2023**, *10*, 428. <https://doi.org/10.3390/photonics10040428>

Received: 25 March 2023

Revised: 7 April 2023

Accepted: 9 April 2023

Published: 10 April 2023



**Copyright:** © 2023 by the authors. Licensee MDPI, Basel, Switzerland. This article is an open access article distributed under the terms and conditions of the Creative Commons Attribution (CC BY) license (<https://creativecommons.org/licenses/by/4.0/>).

freedom for fine-tuning the waveguide dispersion. It has been shown that, by depositing ALD HfO<sub>2</sub> ( $n = 2.03$ ) on the SiN waveguides, more anomalous dispersion can be applied to the waveguide [16], while the GVD of SiN waveguides can be adjusted from normal to anomalous regimes by coating with tellurium oxide (TeO<sub>2</sub>) thin films [17]. A more recent work theoretically demonstrates the potential of near-zero dispersion in silica glass microspheres with micron-scale germanosilicate (GeO<sub>2</sub>) coating [18], which benefits the degenerate four-wave mixing (FWM) processes. Among all the potentials for ALD, alumina (Al<sub>2</sub>O<sub>3</sub>) thin-film coating is the most promising candidate, due to its relatively low loss in the telecom spectral range [19]. However, previous studies have mainly focused on verifying the waveguide dispersion using silicon- or silica-based waveguides/resonators [19,20], and the extent to which dispersion tailoring can be achieved using ALD remains limited.

In this study, we explore the waveguide dispersion by depositing ALD layers onto SiN waveguide resonators by varying cladding materials and thicknesses. Compared to the conventional silicon-based waveguide, SiN is a promising material for nonlinear photonics owing to its relatively large bandgap. Our work has yielded several new achievements. First, we show the capability to adjust dispersion by depositing ALD HfO<sub>2</sub> or Al<sub>2</sub>O<sub>3</sub> cladding layers on top of SiN waveguide resonators. The ALD process shows no impact on the waveguide loss, and therefore the quality (Q) factor remains unchanged. Second, we demonstrate dispersion tailoring by adjusting the ALD thickness for both HfO<sub>2</sub> and Al<sub>2</sub>O<sub>3</sub>; this demonstration is in qualitative agreement with the finite-difference time-domain (FDTD) simulation. This exhibits the flexibility of dispersion engineering. Third, for the first time, the SiN waveguide dispersion can be tuned from normal to anomalous by increasing the thickness of ALD Al<sub>2</sub>O<sub>3</sub>, thereby enabling the initiation of nonlinear mechanism [2,4,6]. Last, we show a low-dispersive SiN waveguide with a GVD value of approximately  $-12$  ps/nm-km by cladding a 50 nm Al<sub>2</sub>O<sub>3</sub> layer. This result suggests the potential for meeting the low dispersion requirements of applications in conventional linear photonics.

## 2. Dispersion Simulation

We first numerically simulated the waveguide dispersion and studied the effect of the ALD thickness. Figure 1 shows the mode profiles and the corresponding waveguide dispersion of the fundamental transverse electric (TE) mode based on the finite element method (FEM, RSoft FemSIM) [21]. Considering air-cladded devices with various core dimensions, as depicted in Figure 1b, it was observed that increasing waveguide heights can cause the waveguide dispersion to transition from normal to zero dispersive regimes, as previously observed in the literature [6–8]. Next, we compared the dispersion for the air-cladded (without cladding) and ALD-cladded devices. The simulation was performed for SiN waveguide resonators with a cross-section of  $500 \text{ nm} \times 3 \text{ }\mu\text{m}$  to avoid unwanted strain-induced cracks from a thick film; a width of  $3 \text{ }\mu\text{m}$  yields better Q factors of waveguide resonators than a width of  $2 \text{ }\mu\text{m}$  [12]. By adjusting the ALD thickness, we can identify that, for both HfO<sub>2</sub> and Al<sub>2</sub>O<sub>3</sub>, thicker ALD films tailor the waveguide dispersion to less normal, low-dispersion regimes. For HfO<sub>2</sub> cladding, the GVD was tuned from  $D = -151$  ps/nm-km for the air-cladded device to  $-92$  ps/nm-km for a 50 nm HfO<sub>2</sub> cladding, while for Al<sub>2</sub>O<sub>3</sub>, the GVD was tuned to  $-46$  ps/nm-km for a 150 nm Al<sub>2</sub>O<sub>3</sub> cladding. Since the waveguide mode is mostly confined in the SiN core layer, it is less effective for dispersion tuning as the ALD thickness is further increased. The GVD with a 250 nm Al<sub>2</sub>O<sub>3</sub> cladding was limited to around  $-35$  ps/nm-km. However, we did not focus on the cladding thickness  $>100$  nm due to the time-consuming ALD process for a thick film. This trend observed in HfO<sub>2</sub> thin films is consistent with that reported by Riemensberger et al. [16]; however, in the case of Al<sub>2</sub>O<sub>3</sub> thin films, the direction in which the waveguide dispersion is tuned is opposite to that confirmed in a silicon strip waveguide [19].

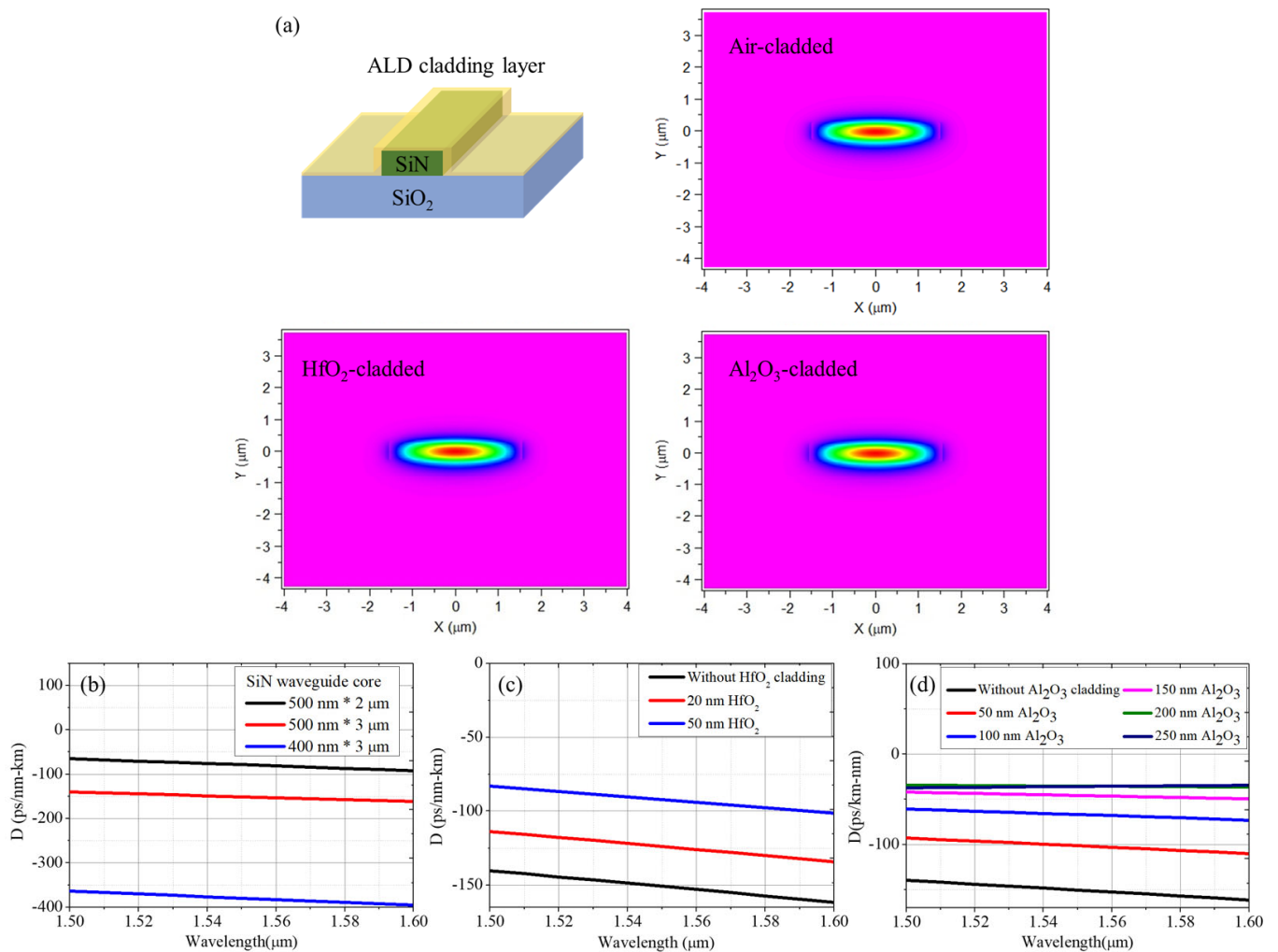


**Figure 1.** (a) Field profiles of the air-cladded and 50 nm ALD-cladded SiN waveguides with a cross-section of  $500 \text{ nm} \times 3 \text{ }\mu\text{m}$ . Waveguide dispersion at around 1550 nm versus the thickness of (b) air cladding, (c)  $\text{HfO}_2$  ALD cladding, and (d)  $\text{Al}_2\text{O}_3$  ALD cladding.

### 3. Device Fabrication and Results

#### 3.1. Device Fabrication and Dispersion Measurement

In fabrication, we first thermally grew a  $2 \text{ }\mu\text{m}$  thick silicon oxide ( $\text{SiO}_2$ ) layer on 4-inch silicon wafers by using a wet oxidation process (SJ-CA1200-D4, SJ, Taiwan). A  $500 \text{ nm}$  SiN film was then deposited via low-pressure chemical vapor deposition (LPCVD, SJ-10301001-1, SJ, Taiwan). After SiN deposition, an i-line ( $365 \text{ nm}$ ) stepper (FPA-3000i5+, Canon, Tokyo, Japan) was used to pattern the waveguide resonators with a positive-tone resist (Sumitomo PFI38). The devices were then dry-etched using a reactive-ion etching tool (Advance Vacuum/Vision 320, Plasma-Therm, St. Petersburg, FL, USA) with a gas ratio  $\text{CHF}_3:\text{O}_2 = 4:1$  at  $150 \text{ W}$  RF power and a process pressure of  $20 \text{ mTorr}$  for  $750 \text{ s}$ . For the ALD-cladded devices, both  $\text{HfO}_2$  and  $\text{Al}_2\text{O}_3$  were deposited by using an ALD reactor (SUNALETM R-200, Picosun, Espoo, Finland) with deposit rate  $\approx 0.1 \text{ nm/cycle}$ . The ALD  $\text{Al}_2\text{O}_3$  layer was processed with a gas ratio  $\text{Al}(\text{CH}_3)_3:\text{H}_2\text{O} = 1:1$  at  $250 \text{ }^\circ\text{C}$ , while the  $\text{HfO}_2$  layer was processed with a gas ratio  $\text{TEMAH}:\text{H}_2\text{O} = 1:4$  at  $200 \text{ }^\circ\text{C}$ . Figure 2 shows the fabrication process and the fabricated devices without and with the ALD cladding.

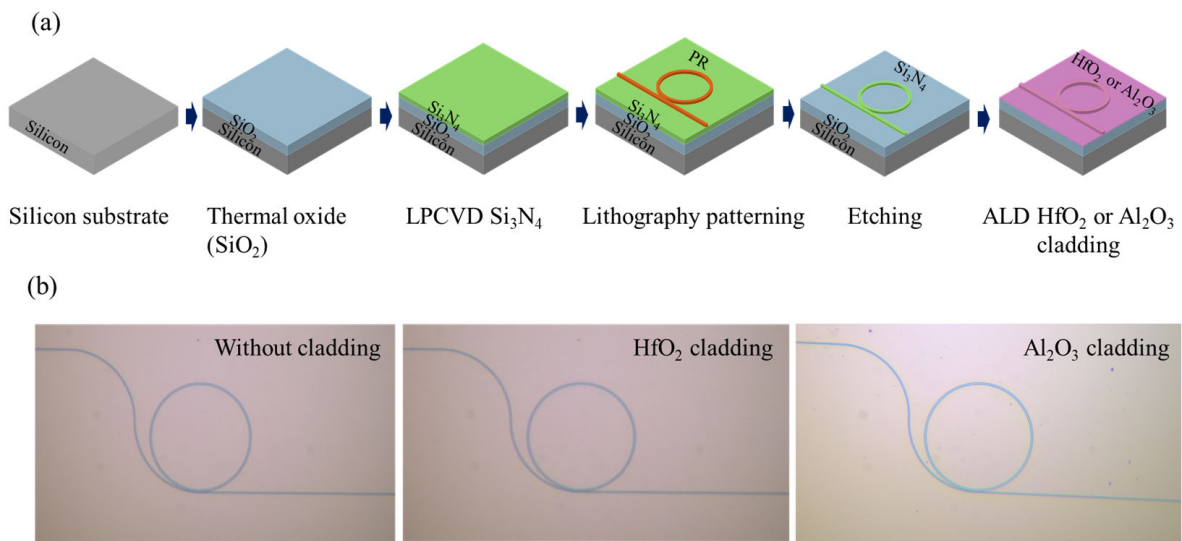


**Figure 2.** (a) Schematics of fabrication processes and (b) images of the fabricated devices without and with the ALD cladding.

The measured transmission spectrum of the exemplary, air-cladded waveguide resonator is shown in Figure 3. The inset shows the corresponding zoomed-in spectrum of the cavity resonance. The waveguide resonator that was demonstrated here only exhibited resonance at the fundamental TE mode while the electric field was injected with polarization parallel to the waveguide. The intrinsic quality factor ( $Q_i$ ) is fitted at around  $1.2 \times 10^5$ .

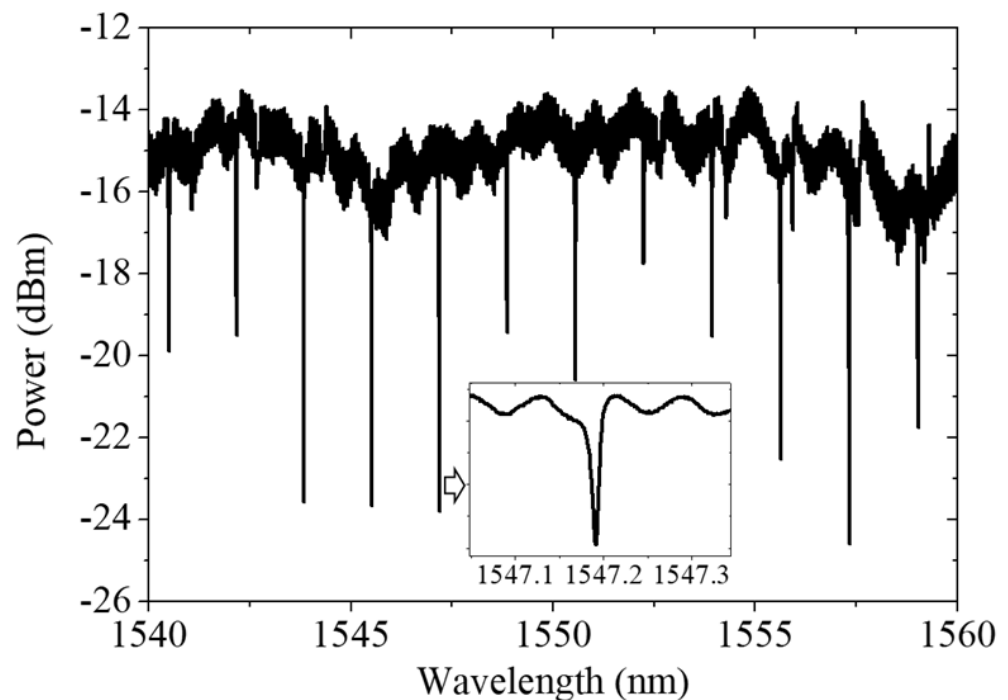


**Figure 3.** The measured optical transmission spectrum of the air-cladded SiN waveguide resonator and the zoomed-in spectrum (inset).

To characterize the waveguide dispersion, we adapted the measurement method from multiple sources [6,14,22] by evaluating the evolution of the adjacent free-spectral-range (*FSR*) of the waveguide resonator. The GVD of waveguide resonator results in

an FSR difference at various wavelengths, and the correspondence can be expressed as follows [6,14,22]:

$$D = \frac{2\pi c}{4\pi^2 \lambda^2 R \cdot FSR^3} \frac{dFSR}{dm} \tag{1}$$

where  $c$  is the speed of light,  $R$  is the radius of the microresonator,  $m$  is the azimuthal mode number, and  $\lambda$  is the optical wavelength. Clearly, larger waveguide dispersion contributes to larger FSR difference of the adjacent FSRs ( $\frac{dFSR}{dm}$ ). However, when measuring a weakly-dispersed waveguide, it is necessary to use high-Q resonators and high-resolution spectra to differentiate the evolution of FSRs. The scheme of the experimental setup is shown in Figure 4. The transmission spectra from 1510 nm to 1590 nm were obtained by using a tunable C-band laser (SANTEC TSL-550, Santec Corporation, Aichi, Japan) and a digital oscilloscope with 100 Mpts memory depth (MSO5204, Rigol, Suzhou, China) for a high-resolution spectrum. A fiber-based interferometry with a 30 m optical path difference was used to generate interference fringes, resulting in a fringe periodicity  $\approx 6.89$  MHz [14].

### Experimental setup

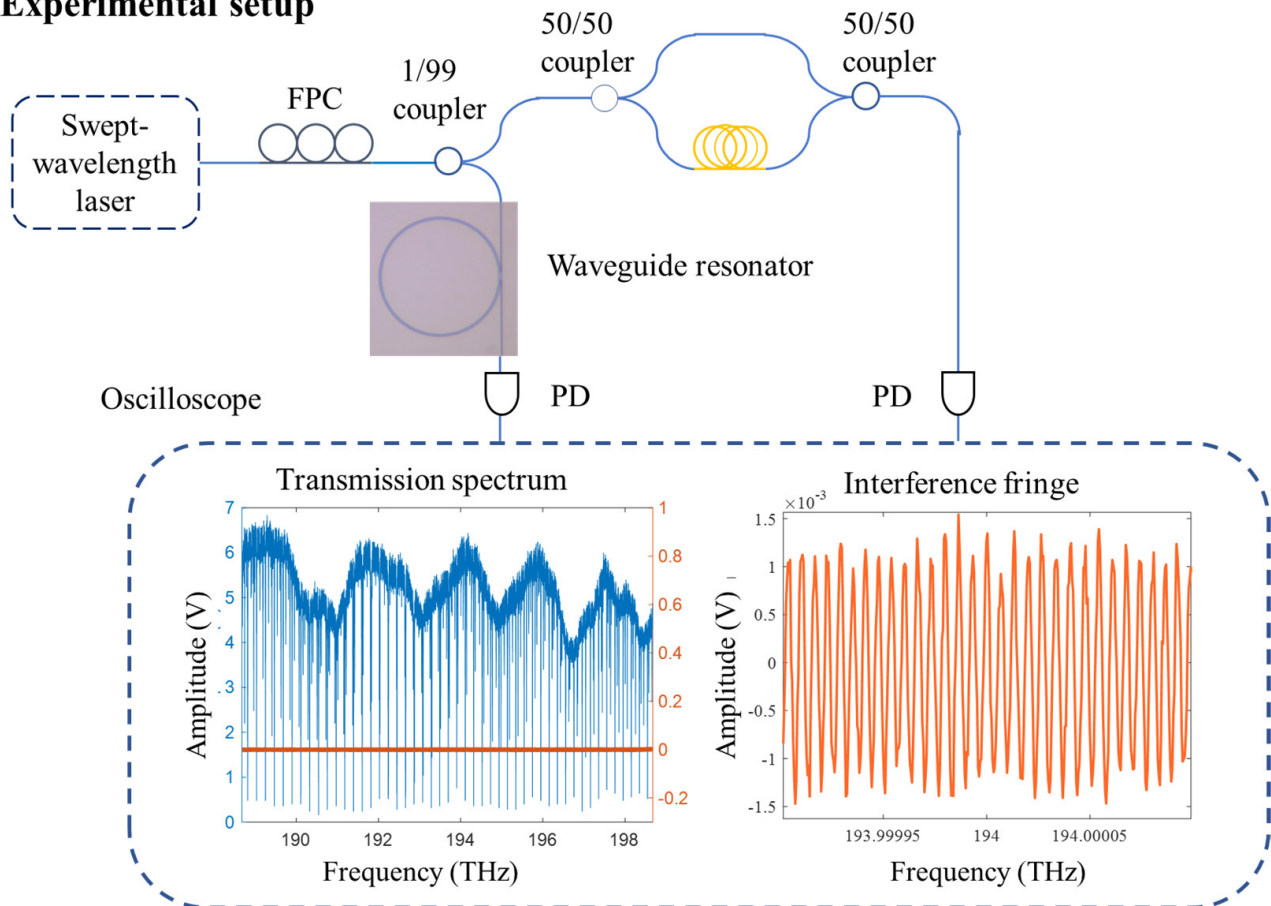


**Figure 4.** Experimental setup for the dispersion measurement.

### 3.2. Results of ALD HfO<sub>2</sub> Cladding

To study the effect of HfO<sub>2</sub> thickness, we gradually increased the thickness of ALD HfO<sub>2</sub> on the same device and measured the corresponding waveguide dispersion values. Figure 5 shows the exemplary recorded transmission spectra for air-cladded, 20 nm, and 50 nm HfO<sub>2</sub> cladded devices. The insets show the exemplary zoomed-in spectra of the interference fringes from the fiber-interferometry system. By extracting the respective resonant frequencies, the evolution of FSRs and the measured waveguide dispersion are shown in Figure 6 for air-cladded, 20 nm, and 50 nm HfO<sub>2</sub> claddings.

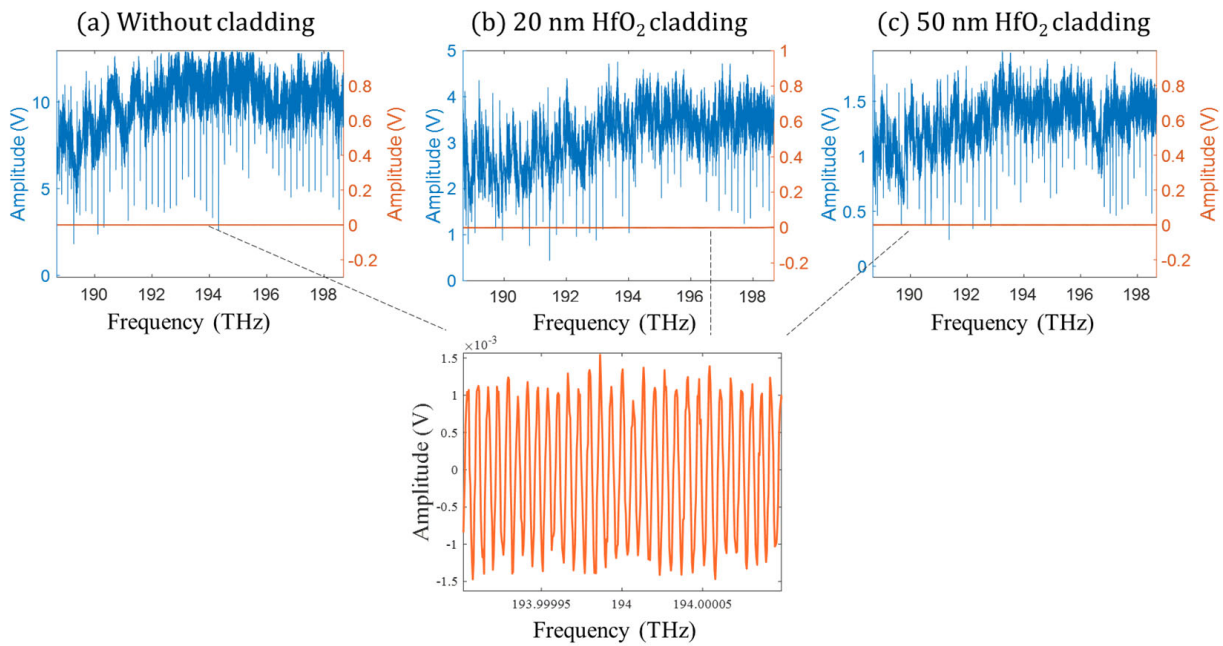


**Figure 5.** Transmission spectra and interference fringes of the (a) air-cladded, (b) 20 nm, and (c) 50 nm ALD-cladded devices.

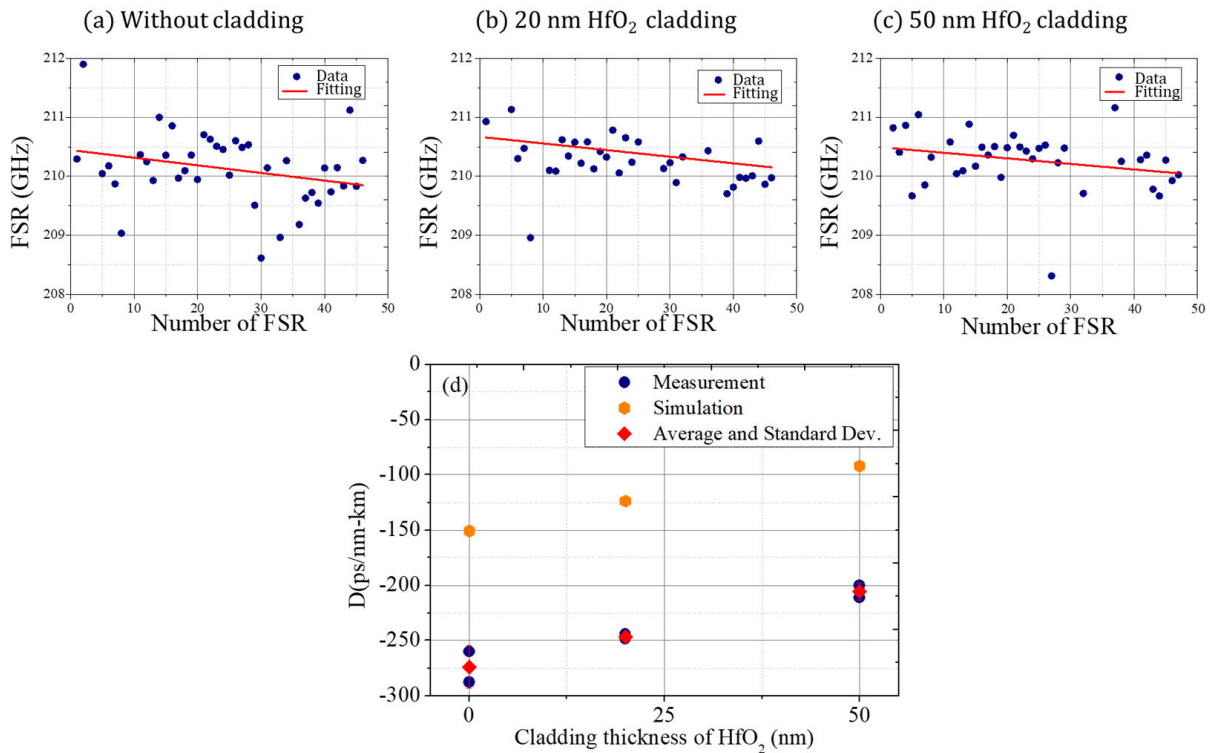


**Figure 6.** Evolution of FSRs for (a) air-cladded, (b) 20 nm, and (c) 50 nm HfO<sub>2</sub> cladded devices. (d) The measured waveguide dispersion versus the cladding thickness of HfO<sub>2</sub> cladding.

The measured waveguide dispersion shows that the GVD can be smoothly tuned, ranging from  $D = -274$  ps/nm-km (with air-cladding) to  $-246$  ps/nm-km (with a 20 nm HfO<sub>2</sub> cladding), and even down to  $-205$  ps/nm-km (with a 50 nm HfO<sub>2</sub> cladding). This qualitatively agrees with the FEM simulation, showing a trend toward zero dispersion as the ALD cladding thickness increases. There is a persistent discrepancy ( $\approx 120$  ps/nm-km) that may be due to the varying material properties of the SiN waveguides or the cladding

materials. We have identified here that the tuning range of up to 70 ps/nm-km can be achieved with a 50 nm cladding thickness; furthermore, it should be emphasized that the dispersion can be finely tuned within this range by accurately controlling the thickness of ALD films.

### 3.3. Results of ALD Al<sub>2</sub>O<sub>3</sub> Cladding

Next, we investigated the effect of ALD Al<sub>2</sub>O<sub>3</sub> cladding. Another SiN waveguide resonator was fabricated using the same fabrication process and layout for characterization. Again, the thickness of ALD Al<sub>2</sub>O<sub>3</sub> was gradually increased, and the corresponding transmission spectra are shown in Figure 7. We can observe that cavity resonances with a high extinction ratio can be realized for thickness of Al<sub>2</sub>O<sub>3</sub> cladding up to 60 nm, which results in close to critical coupling. This also implies that the ALD layer does not affect the waveguide loss of the microresonators. By extracting the respective resonant frequencies, the evolution of FSRs and the measured waveguide dispersion are shown in Figure 8 for air-cladded, 20 nm, 50 nm, and 60 nm Al<sub>2</sub>O<sub>3</sub> claddings. The measured GVD was tuned from −213 ps/nm-km (with air-cladding) to −114 ps/nm-km (with a 20 nm Al<sub>2</sub>O<sub>3</sub> cladding), and even down to −12 ps/nm-km (with a 50 nm Al<sub>2</sub>O<sub>3</sub> cladding), offering the opportunity for realizing a low-dispersive waveguide. In addition, in order to achieve anomalous dispersion for nonlinear applications [2,4,6], we further increased the thickness of Al<sub>2</sub>O<sub>3</sub> cladding to 60 nm, resulting in an anomalous GVD value of 46 ps/nm/km. This identification in SiN waveguides demonstrates an opposite trend to that observed in a silicon strip waveguide [19], in which the dispersion of a thicker ALD layer is tuned to less anomalous dispersion regimes. It also represents the first experimental evidence of this effect in a SiN waveguide, which opens up the potential for SiN-based nonlinear photonics. Increasing the thickness of the Al<sub>2</sub>O<sub>3</sub> cladding tailors the dispersion to the anomalous dispersion regime, which agrees qualitatively with the simulated GVD, as indicated by the orange dots in Figure 8. Additionally, we observe that ALD thickness control provides more effective tuning capability than the theoretical one. This difference in tuning capability may be attributed to difference in the material properties used in the simulation.

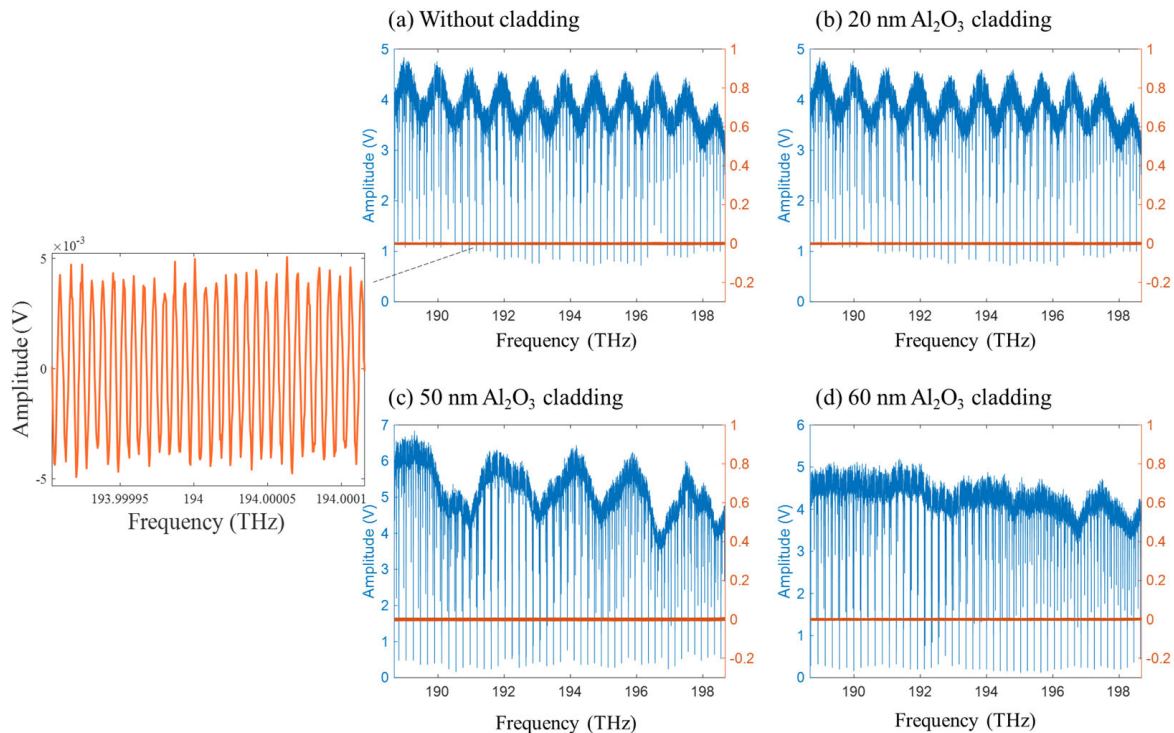


**Figure 7.** Transmission spectra and interference fringes (orange lines) of the (a) air-cladded, (b) 20 nm, (c) 50 nm, and (d) 60 nm ALD-cladded devices.

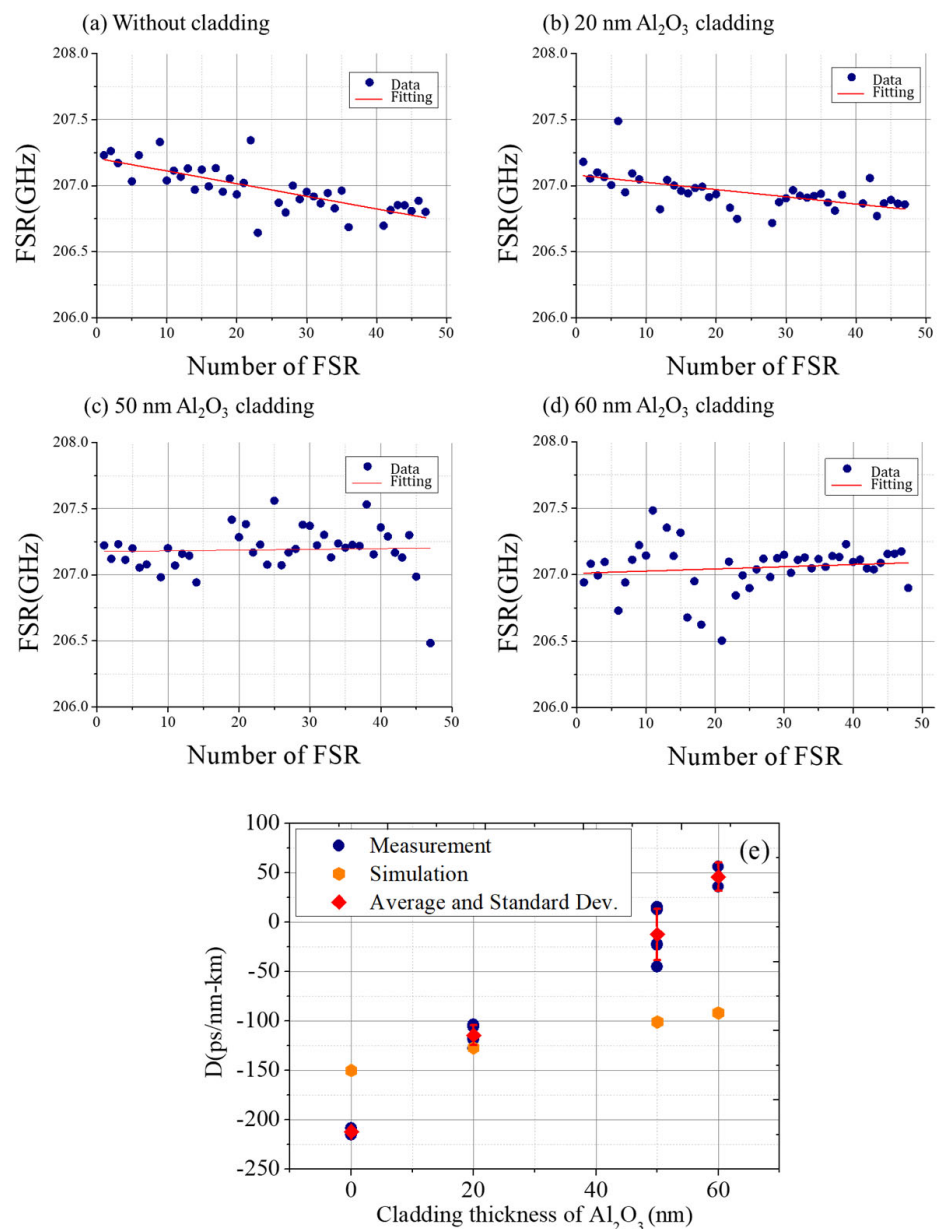


**Figure 8.** Evolution of FSRs for (a) air-cladded, (b) 20 nm, (c) 50 nm, and (d) 60 nm Al<sub>2</sub>O<sub>3</sub> cladded devices. (e) The measured waveguide dispersion versus the cladding thickness of Al<sub>2</sub>O<sub>3</sub> cladding.

#### 4. Discussion

Here, we emphasize our findings on the effect of ALD layers on quality factors. As mentioned previously, the ALD process has been found to have no significant impact on the waveguide loss, as indicated by the unchanged extinction ratio of the resonances. To further address this issue, the intrinsic Q factors were extracted from the measured spectra around 1550 nm by fitting the individual resonances, and the coupling condition was estimated by the drop-port geometry [23], showing under-coupling. The mode crossing points with high-order modes were ignored to avoid local dispersion change. Figure 9 shows the fitted intrinsic Q factors for both ALD HfO<sub>2</sub> and Al<sub>2</sub>O<sub>3</sub> claddings. Examining the results of both layers shows that the intrinsic Q factors remain unchanged across the various ALD thicknesses studied. The analysis reveals that there is only a  $\leq 10\%$  variation within the standard deviation of the measurements. This suggests that the ALD process has a negligible effect on the waveguide loss, and consequently, the Q factors.

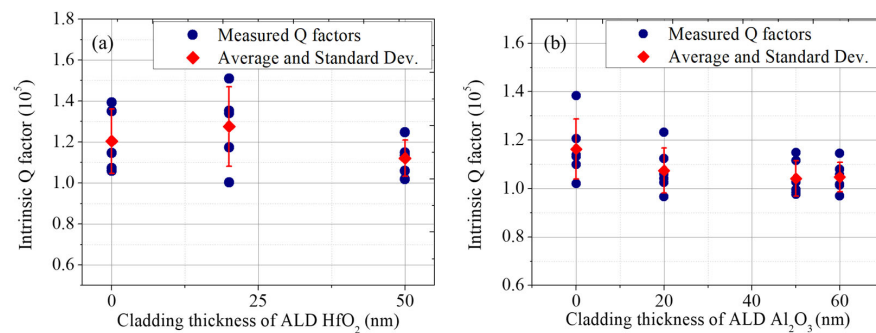


**Figure 9.** Intrinsic Q factors versus the ALD thickness for (a)  $\text{HfO}_2$  and (b)  $\text{Al}_2\text{O}_3$ .

It is worth noting that the excellent step coverage of ALD films allows for precise deposition in narrow gaps. Therefore, when using 60 nm ALD deposition to fill the adapted 400 nm gap between bus- and resonator-waveguides, it should not be completely filled. Moreover, due to the effectively larger waveguide mode for a 60 nm ALD film, the loaded Q is slightly decreased by a factor of approximately 1.2 when there is stronger coupling between the bus- and resonator-waveguides.

Lastly, this technique can also be utilized to customize the waveguide dispersion locally. This can be achieved by selectively covering the ALD with a lithography and lift-off process. Since ALD allows deposition at low temperatures, even as low as 100–150 °C, it prevents the outgassing and hard-baking of photoresist layers [24]. This makes it possible to use a lift-off process to selectively form a covering of ALD layers without the need for an etching process [24,25], preventing the potential damage to critical layers, such as the waveguide core. This approach relieves the risk of causing surface roughness during the fabrication process.

## 5. Conclusions

In conclusion, our work sheds light on dispersion engineering of waveguide resonators through the use of various ALD layers and thicknesses. Both  $\text{HfO}_2$  and  $\text{Al}_2\text{O}_3$  cladding layers offer precise control over the deposited thickness, providing a fine-tuning capability for tailoring waveguide dispersion. Ultra-low dispersive SiN waveguide with a GVD value  $\approx -12$  ps/nm-km is demonstrated with a 50 nm  $\text{Al}_2\text{O}_3$  cladding, while the dispersion can be further tailored to the anomalous dispersion regime by a 60 nm  $\text{Al}_2\text{O}_3$  cladding. Furthermore, the ALD cladding layers show negligible impact on the waveguide loss and, therefore, the Q factors. This demonstration realizes the potential of SiN-based waveguides for applications in both linear and nonlinear photonics.

**Author Contributions:** Conceptualization and methodology, P.-H.W.; investigation, N.-L.H. and K.-L.H.; data curation, N.-L.H.; writing—original draft preparation, P.-H.W.; writing—review and editing, P.-H.W. and N.-L.H. All authors have read and agreed to the published version of the manuscript.

**Funding:** This work is supported by the National Science and Technology Council (NSTC), Taiwan, under grant numbers 111-2221-E-008-026 and 111-2622-8-008-007.

**Institutional Review Board Statement:** Not applicable.

**Informed Consent Statement:** Not applicable.

**Data Availability Statement:** Data underlying the results presented in this paper are not publicly available at this time but may be obtained from the authors upon reasonable request.

**Acknowledgments:** P.-H.W. acknowledge the research financial support from the National Science and Technology Council (NSTC), Taiwan, under grant numbers 111-2221-E-008-026 and 111-2622-8-008-007. The authors thank the Nano Facility Center (NFC) of National Yang Ming Chiao Tung University (YMCT), Taiwan, for LPCVD  $\text{Si}_3\text{N}_4$  layer preparation, Taiwan Semiconductor Research Institute (TSRI) for stepper lithography process and RSoft tool support, and Optical Sciences Center (OSC) of National Central University (NCU), Taiwan, for fabrication support.

**Conflicts of Interest:** The authors declare no conflict of interest.

## References

1. Ghatak, A.; Thyagarajan, K. *Introduction to Fiber Optics*; Cambridge University Press: Cambridge, CA, USA, 1998.
2. Agrawal, G.P. *Nonlinear Fiber Optics*, 5th ed.; Springer: New York, NY, USA, 2013.
3. Chen, L.; Xu, Q.; Lipson, M. Understanding dispersion and waveguiding in silicon wire waveguides. *Opt. Express* **2008**, *16*, 14986–14991.
4. Peccianti, M.; Assanto, G. Nonlinear optical phenomena in silicon waveguides: Modeling and applications. *IEEE J. Quantum Electron.* **2016**, *52*, 1–18.
5. Ellis, A.D. Dispersion management for high-speed optical communications. *IEEE J. Sel. Top. Quantum Electron.* **2002**, *8*, 418–431.
6. Hong, Y.; Hong, Y.; Hong, J.; Lu, G.-W. Dispersion optimization of silicon nitride waveguides for efficient four-wave mixing. *Photonics* **2021**, *8*, 161. [[CrossRef](#)]
7. Kordts, A.; Pfeiffer, M.H.; Guo, H.; Brasch, V.; Kippenberg, T.J. Higher order mode suppression in high-Q anomalous dispersion SiN microresonators for temporal dissipative Kerr soliton formation. *Opt. Lett.* **2016**, *41*, 452–455. [[CrossRef](#)]
8. Chavez Boggio, J.M.; Bodenmüller, D.; Fremberg, T.; Haynes, R.; Roth, M.M.; Eisermann, R.; Lisker, M.; Zimmermann, L.; Böhm, M. Dispersion engineered silicon nitride waveguides by geometrical and refractive-index optimization. *J. Opt. Soc. Am. B* **2014**, *31*, 2846–2857. [[CrossRef](#)]
9. Wang, Y.; Zhang, M.; Lu, L.; Li, M.; Wang, J.; Zhou, F.; Dai, J.; Deng, L.; Liu, D. Ultra-flat and broad optical frequency combs generation based on novel dispersion-flattened double-slot microring resonator. *Appl. Phys. A* **2016**, *122*, 11. [[CrossRef](#)]
10. Guo, Y.; Jafari, Z.; Agarwal, A.M.; Kimerling, L.C.; Li, G.; Michel, J.; Zhang, L. Bilayer dispersion-flattened waveguides with four zero-dispersion wavelengths. *Opt. Lett.* **2016**, *41*, 4939–4942. [[CrossRef](#)]
11. Pfeiffer, M.H.; Kordts, A.; Brasch, V.; Zervas, M.; Geiselmann, M.; Jost, J.D.; Kippenberg, T.J. Photonic Damascene process for integrated high-Q microresonator based nonlinear photonics. *Optica* **2016**, *3*, 20–25. [[CrossRef](#)]
12. Xuan, Y.; Liu, Y.; Varghese, L.T.; Metcalf, A.J.; Xue, X.; Wang, P.-H.; Han, K.; Jaramillo-Villegas, J.A.; Al Noman, A.; Wang, C.; et al. High-Q silicon nitride microresonators exhibiting low-power frequency comb initiation. *Optica* **2016**, *3*, 1171–1180. [[CrossRef](#)]
13. Gondarenko, A.; Levy, J.S.; Lipson, M. High confinement micron-scale silicon nitride high Q ring resonator. *Opt. Express* **2009**, *17*, 11366–11370. [[CrossRef](#)] [[PubMed](#)]
14. Wang, S.-P.; Lee, T.-H.; Chen, Y.-Y.; Wang, P.-H. Dispersion engineering of silicon nitride microresonators via reconstructable SU-8 polymer cladding. *Micromachines* **2022**, *13*, 454. [[CrossRef](#)] [[PubMed](#)]
15. Khanna, A.; Subramanian, A.Z.; Häyrynen, M.; Selvaraja, S.; Verheyen, P.; Van Thourhout, D.; Honkanen, S.; Lipsanen, H.; Baets, R. Impact of ALD grown passivation layers on silicon nitride based integrated optic devices for very-near-infrared wavelengths. *Opt. Express* **2014**, *22*, 5684–5692. [[CrossRef](#)] [[PubMed](#)]
16. Riemensberger, J.; Hartinger, K.; Herr, T.; Brasch, V.; Holzwarth, R.; Kippenberg, T.J. Dispersion engineering of thick high-Q silicon nitride ring-resonators via atomic layer deposition. *Opt. Express* **2012**, *20*, 27661–27669. [[CrossRef](#)]
17. Kiani, K.M.; Mbonde, H.M.; Frankis, H.C.; Mateman, R.; Leinse, A.; Knights, A.P.; Bradley, J.D.B. Four-wave mixing in High-Q tellurium-oxide-coated silicon nitride microring resonators. *OSA Continuum* **2020**, *3*, 3497–3507. [[CrossRef](#)]
18. Marisova, M.P.; Andrianov, A.V.; Leuchs, G.; Anashkina, E.A. Dispersion tailoring and four-wave mixing in silica microspheres with germanosilicate coating. *Photonics* **2021**, *8*, 473. [[CrossRef](#)]
19. Guo, K.; Christensen, J.B.; Shi, X.; Christensen, E.N.; Lin, L.; Ding, Y.; Ou, H.; Rottwitt, K. Experimentally validated dispersion tailoring in a silicon strip waveguide with alumina thin-film coating. *IEEE Photonics J.* **2018**, *10*, 1–8. [[CrossRef](#)]
20. Inga, M.; Fujii, L.; Filho, J.M.C.S.; Palhares, J.H.Q.; Ferlauto, A.S.; Marques, F.C.; Alegre, T.P.M.; Wiederhecker, G. Alumina coating for dispersion management in ultra-high Q microresonators. *APL Photonics* **2020**, *5*, 116107. [[CrossRef](#)]
21. *RSoft FemSIM*, RSoft Products; Synopsys, Inc.: Mountain View, CA, USA, 2007.
22. Fujii, S.; Tanabe, T. Dispersion engineering and measurement of whispering gallery mode microresonator for Kerr frequency comb generation. *Nanophotonics* **2020**, *9*, 1087–1104. [[CrossRef](#)]
23. Wang, P.H.; Lee, T.H.; Huang, W.H. Fabrication of tapered waveguides by i-line UV lithography for flexible coupling control. *Opt. Express* **2023**, *31*, 4281–4290. [[CrossRef](#)]
24. Mackus, A.J.M.; Bol, A.A.; Kessels, W.M.M. The use of atomic layer deposition in advanced nanopatterning. *Nanoscale* **2014**, *6*, 10941–10960. [[CrossRef](#)] [[PubMed](#)]
25. Biercuk, M.J.; Monsma, D.J.; Marcus, C.M.; Becker, J.S.; Gordon, R.G. Low-temperature atomic-layer-deposition lift-off method for microelectronic and nanoelectronic applications. *Appl. Phys. Lett.* **2003**, *83*, 2405–2407. [[CrossRef](#)]

**Disclaimer/Publisher’s Note:** The statements, opinions and data contained in all publications are solely those of the individual author(s) and contributor(s) and not of MDPI and/or the editor(s). MDPI and/or the editor(s) disclaim responsibility for any injury to people or property resulting from any ideas, methods, instructions or products referred to in the content.